Quantum coherence and classical chaos in a pulsed parametric oscillator with a Kerr nonlinearity

G. J. Milburn
Department of Physics, University of Queensland, St. Lucia 4072, Australia

C. A. Holmes
Department of Mathematics, University of Queensland, St. Lucia 4072, Australia
(Received 15 January 1991)

We consider a parametric amplifier driven by a periodically pulsed pump field inside a cavity containing a Kerr nonlinearity. The dynamics of the device is modeled as a kicked nonlinear system. The pulsed parametric amplifier constitutes the kick. In between kicks the dynamics is determined by the Kerr nonlinearity and damping. In the absence of damping, a classical description of the device exhibits a rich phase-space structure including fixed points of multiple period and chaos. We contrast the classical behavior of the mean intensity with that predicted by quantum dynamics. The mean photon number inside the cavity is shown to undergo regular collapse and revival in the regular region of the phase space and irregular revivals in the chaotic region. When damping is included, the quantum recurrences are rapidly suppressed, and the classical behavior is restored. In this case a stable steady state is possible. The damping represents the effect of photon-number measurements on the system. We also discuss the photon statistics in the steady state.

PACS number(s): 42.50.Tj, 42.65.Ky, 05.45.+b

I. INTRODUCTION

Classical chaotic behavior is drastically modified if not eliminated by quantization. For example, the energy diffusion exhibited by the kicked rotor in the globally chaotic region does not survive in the quantum model [1,2]. The diffusion is suppressed due to complicated interference effects reminiscent of Anderson localization [3]. In this phenomenon we see the signature of quantum coherence, a feature at the heart of the less intuitive aspects of quantum mechanics. However, the quantum behavior can reflect the classical dynamics, be it regular or chaotic. This is quite evident in the dynamics of periodically kicked nonlinear Hamiltonian systems. Early work focused on the change in the quasienergy statistics of the quantum problem as the corresponding classical realization moved into the chaotic region [4]. More recently it has been shown that the classical transition to chaos is reflected in the appearance of irregular collapses and revivals in the evolution of certain moments [5].

It has proved very difficult to find experimental realizations of kicked Hamiltonian models that exhibit chaos. The one example to date is the microwave ionization of hydrogen, where the quantum suppression of diffusion appears to have been confirmed by experiment [6]. The major problem in the search for such realizations is the unavoidable presence of dissipation. At the very least, information must be extracted from the system and this measurement necessarily entails introducing noise and possibly damping into the quantum dynamics. It is well known that quantum coherence effects are extremely sensitive to such nonunitary effects and may not occur at all if the scale of the system (as measured, say, in terms of the initial energy) is too large. It is in this context that quantum optics offers some hope. At optical frequencies the temperature of the environment may be taken as zero and all that remains is the unavoidable coupling to the vacuum. Further, optical nonlinearities exist that enable direct realization of simple nonlinear Hamiltonians, for example the twist map in the case of a Kerr nonlinearity.

In this paper we discuss a simple optical system that realizes the perturbed twist map [7]. The system may be modeled classically or quantum mechanically with dissipation included in both cases. Consider a single-mode field propagating in a cavity (or fiber) containing a Kerr medium (which exhibits an intensity-dependent refractive index). This single-mode field is well described in terms of a simple harmonic oscillator. The effect of the nonlinearity is then to introduce an energy-dependent phase shift of the oscillator's complex amplitude, that is, a rotational sheer in the phase plane [8]. The mode is periodically "kicked" by parametric amplification, which for a very short time turns the origin in phase space into a hyperbolic fixed point, thus stretching and shrinking the phase plane in orthogonal directions. Such devices produce squeezed states and now operate successfully in a number of laboratories [9]. This device might be constructed as a cavity containing the Kerr medium and a parametric amplifier pumped by an intense periodically pulsed field external to the cavity. See Fig. 1.

The classical dynamics of this system exhibits a rich structure of regular and chaotic motion, with the amplifier gain being the control parameter. The phase space is divided into two regions: bounded but possibly chaotic motion and unbounded motion some distance form the origin where trajectories escape to infinity. We discuss the classical motion in detail in Sec. II. When small dissipation is included, the stable fixed points become attractors and a stable steady state is possible. With large damping and large parametric gain the presence of a strange attractor is apparent and consequently the model exhibits a transition to a dissipative chaotic

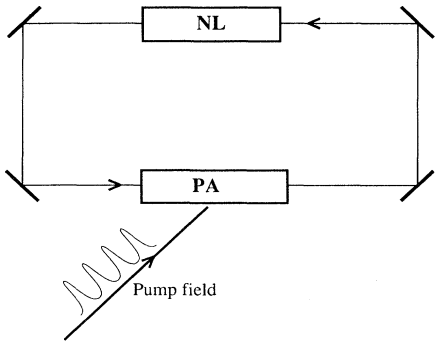

FIG. 1. Schematic representation of the model discussed in this paper. The box labeled NL represents the Kerr medium. The box labeled PA represents a parametric amplifier, pumped by a pulsed field.

structure. In order to compare the classical and quantum models we consider the mean energy of the classical model for an initial distribution of position and momentum taken to have the same spread as characterizes an oscillator coherent state.

In Sec. III we consider the quantum theory of the model for initial coherent states (including the vacuum). We show that the mean photon number exhibits a collapse and revival sequence. That is to say, the mean photon number oscillates with an amplitude that initially decays but that periodically or quasiperiodically returns close to the initial amplitude. For initial states localized in the regular region of phase space these revivals are quite regular, almost periodic. However, in the irregular region the revivals become quite irregular. Damping is included in the quantum model using the method described in Ref. [10]. We find as expected that typical quantum recurrence features are rapidly suppressed and the mean intensity approaches that expected from the classical description. The model used for damping may be equivalently interpreted as due to continual photon counting measurements being made on the intracavity field. Thus we also describe in a very natural way the effect of measurement on a quantum system that is classically chaotic.

In the absence of dissipation, the dynamics in the period between kicks is determined by the Hamiltonian [8]

$$H_{\rm NL}=\frac{\chi}{2}(a^\dagger)^2a^2 , \tag{1.1}$$

where χ is proportional to the third-order nonlinear susceptibility and $a,a^\dagger$ are the complex amplitude operators for the field. These operators obey the commutation relations $[a,a^\dagger]=1$. To enable a more direct classical representation it is useful to write the complex amplitude operators in terms of dimensionless position and momentum operators (or quadrature phase operators) $\hat{X}_1$ and $\hat{X}_2$ by

$$a=\hat{X}_1+i\hat{X}_2 . \tag{1.2}$$

The Heisenberg equation of motion for a is

$$\frac{da}{dt}=-i\chi a^\dagger aa \tag{1.3}$$

(units have been chosen such that $\hbar=1$). As the energy operator $a^\dagger a$ is a constant of motion, Eq. (3) has the solution

$$a(t)=e^{-i\mu a^\dagger a}a(0) , \tag{1.4}$$

where $\mu=\chi t$. Equation (1.4) describes an energy-dependent phase shift.

The parametric kicks are described by the Hamiltonian

$$H_K=i\hbar\frac{\kappa}{2}[(a^\dagger)^2-a^2] . \tag{1.5}$$

In writing this Hamiltonian it is assumed that the pump carrier frequency is twice that of the intracavity field and a transformation to the interaction picture has been made. The coupling constant κ is the product of the pump field amplitude and the second-order nonlinearity in the parametric gain medium. Thus κ is increased by increasing the pump amplitude. The Heisenberg equation of motion following from Eq. (1.5) is

$$\frac{da}{dt}=\kappa a^\dagger \tag{1.6}$$

and a corresponding Hermitian conjugate equation. The solution is

$$a(t)=a(0)\cosh(s)+a^\dagger(0)\sinh(s) , \tag{1.7}$$

where $s=\kappa t$. In the case of a pulsed pump field, s is determined by the integrated time-dependent amplitude of the pump.

We will assume that the pump is turned on and off so rapidly compared to the free dynamics that the Hamiltonian describing the parametric process may be approximated by

$$H_{\rm PA}=H_K\sum_{n=-\infty}^{\infty}\delta(t-n\tau) , \tag{1.8}$$

where τ is the period of free evolution between each pump pulse. The effect of the parametric process is then from Eq. (1.7) given by

$$a(t_n^+)=a(t_n^-)\cosh r+a^\dagger(t_n^-)\sinh r , \tag{1.9}$$

where t_n^+ (t_n^-) is the time just after (before) the passage of the nth pulse and r is the effective parametric constant for the pulse.

Equation (1.7) may be written in terms of the Hermitian phase-space operators:

$$\begin{aligned}\hat{X}_1(t_n^+)&=e^r\hat{X}_1(t_n^-)\equiv g\hat{X}_1(t_n^-) ,\\ \hat{X}_2(t_n^+)&=e^{-r}\hat{X}_2(t_n^-)\equiv\frac{1}{g}\hat{X}_2(t_n^-) ,\end{aligned} \tag{1.10}$$

where $g\equiv e^r$ is the parametric gain.

II. THE CLASSICAL MODEL

There are a number of ways to give a classical description of the model presented above. We adopt the procedure of replacing the operators $(a,a^\dagger)$ and $(\hat{X}_1,\hat{X}_2)$ by classical commuting phase-space variables (α,α^*) and (X_1,X_2) [11]. The classical Hamiltonian constructed

from the quantum Hamiltonian by this substitution will give the correct classical equations of motion (Hamilton's equations), at least up to constant frequency shifts that scale to zero in the semiclassical limit. The classical analogs of Eqs. (1.3) and (1.7) are then

$$\frac{d\alpha(t)}{dt}=-i\chi|\alpha|^2\alpha-\frac{\gamma'}{2}\alpha \tag{2.1}$$

for the free evolution, while the effect of the parametric kicks is given by

$$\alpha(t_n^+)-\alpha(t_n^-)\cosh(r)+\alpha^*(t_n^-)\sinh(r)\ , \tag{2.2}$$

where $\alpha=X_1+iX_2$. Note that we have explicitly allowed for the possibility that dissipation may be present over the period of free evolution in Eq. (2.1) by including the decay term proportional to γ'. The solution of Eq. (2.1) is

$$\alpha(\tau)=\alpha(0)\exp\left[-\frac{\gamma}{2}-i\phi|\alpha(0)|^2\right]\ , \tag{2.3}$$

where

$$\phi=\frac{\mu}{\gamma}(1-e^{-\gamma})\ , \tag{2.4}$$

where the damping constant γ is defined by $\gamma=\gamma'\tau$. Combining Eqs. (2.2) and (2.3) we find that the classical dynamics from just after one kick to just after the next kick is determined by the map

$$X_1'=ge^{-\gamma/2}[\cos(\phi R^2)X_1+\sin(\phi R^2)X_2]\ , \tag{2.5}$$

$$X_2'=\frac{1}{g}e^{-\gamma/2}[-\sin(\phi R^2)X_1+\cos(\phi R^2)X_2]\ , \tag{2.6}$$

where $R^2=X_1^2+X_2^2$.

We first discuss the case of no dissipation ($\gamma=0$) and then $\phi=\mu=\chi\tau$. The origin is an unstable critical point for all nonzero values of r (μ is simply a scaling parameter). There are two other critical points in the disk $R<\sqrt{\pi/\mu}$ given by

$$\mu R_{0+}^2=\cos^{-1}\left[\frac{1}{\cosh r}\right]\ , \tag{2.7}$$

$$\tan(\theta_+)=-\exp(-r)\ , \tag{2.8}$$

and in each annular region

$$\left[\frac{(2n-1)\pi}{\mu}\right]^{1/2}<R<\left[\frac{(2n+1)\pi}{\mu}\right]^{1/2}\ ,\qquad n=1,2,3,\ldots \tag{2.9}$$

there are four critical points given by

$$\mu R_{n\pm}^2=2n\pi\pm\cos^{-1}\left[\frac{1}{\cosh r}\right],\quad n=1,2,3,\ldots \tag{2.10}$$

$$\tan\theta_\pm=\mp e^{pr}\ . \tag{2.11}$$

Since $\theta_\pm$ is independent of n, these lie on one of the four radial lines

$$\theta=\tan^{-1}(e^{-r})\ , \tag{2.12}$$

$$\theta=\pi+\tan^{-1}(e^{-r})\ , \tag{2.13}$$

$$\theta=-\tan^{-1}(e^{-r})\ , \tag{2.14}$$

$$\theta=\pi-\tan^{-1}(e^{-r})\ , \tag{2.15}$$

All the critical points denoted (R_{n-},θ_-), $n=1,2,3,\ldots$ (there are two for each value of n placed symmetrically about the origin) are unstable, whereas those denoted (R_{n+},θ_+), $n=0,1,2,\ldots$ are unstable (or stable) only if

$$P(n,r)=\left[\pi+\cos^{-1}\left[\frac{1}{\cosh r}\right]\right]\sinh r>\ (\text{or}\ <)2\ . \tag{2.16}$$

From this it follows that for any fixed nonzero value of r there is some value of n, n_c, say, such that for $n\geq n_c$ (R_{n+},θ_+) is unstable and for $n<n_c$, (R_{n+},θ_+) is stable. As r increases from zero, passing through the critical values r_{n_s}, given by $P(n,r_{n_s})=2$, the number of stable critical points decreases until for $r<r_{0_s}$ all the critical points are unstable.

However, even if (R_{n+},θ_+) is stable, this is no guarantee that solutions nearby will stay nearby since for all nonzero values of r the system is chaotic. To obtain some kind of estimate for the onset of chaos we follow the work of Greene [12]. If we take action angle variables in the vicinity of the stable critical points and including only terms to first order in the action, then the absence of damping ensures that the action is unchanged while the angle undergoes a translation by $2\pi\phi$, where ϕ is a constant called the rotation number. Greene observed that the final barrier to global stochasticity disappears when $\phi=\frac{1}{6}$. For the critical point (R_{n+},θ_+), $\phi=\frac{1}{6}$ when $r=r_{n_c}$, where $P(n,r_{n_c})=(\sqrt{5}+1)/\sqrt{5}$. Thus for $r<r_{n_c}$ the critical point (R_{n+},θ_+) (which is stable $r_{n_c}<r_{n_s}$) is only locally chaotic. That is to say, bounding Kol'mogorov-Arnol'd-Moser (KAM) tori, or at least islets of stability, will be found nearby. (Note, however, that $r-r_{n_c}$ is only an approximate upper bound for the transition to global chaos.) For $r_{n_c}<r<{}_{n_s}$ it is globally chaotic while still being stable. Since $r_{1_c}<r_{1_s}<r_{0_c}<r_{0_s}$ as r increases, the critical points in the first annular region become unstable before global chaos develops in the vicinity of (R_{0+},θ_+). However, this ordering is not preserved for large n.

Figures 2 and 3 show phase portraits for the map. In Fig. 2, $r_{2_s}<r<r_{1_c}$ (r close to r_{1_c}) so that (R_{0+},θ_+) and (R_{1+},θ_+) are stable and (R_{0+},θ_+) is locally chaotic, while all the other critical points are unstable. Since r is close to r_{1_c} and r_{1_c} is only an upper bound for the transition to global chaos, we do not expect to find much regular behavior near (R_{0+},θ_+). However, regular behavior near (R_{1+},θ_+) is evident as is the period two critical point farther out. In Fig. 3, $r_{0_s}<r<r_{1_s}$ so that (R_{1+},θ_+) is the only stable critical point and it is locally chaotic.

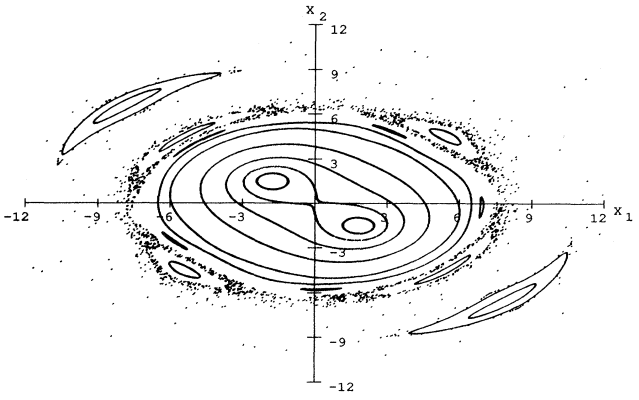

FIG. 2. Phase portrait of the classical map in the absence of dissipation. $g=1.2, \mu=0.01\pi$.

When dissipation is present but $\gamma<2r$, critical points continue to exist, in the same region of phase space as for the undamped case, and are given by

$$\mu R_{0+}=\cos^{-1}\left[\frac{\cosh(\gamma/2)}{\cosh r}\right],$$

$$\mu R_{n\pm}^2=2n\pi\pm\cos^{-1}\left[\frac{\cosh(\gamma/2)}{\cosh r}\right], \quad n=1,2,\ldots$$

$$\tan\theta_{\pm}=\pm e^{-r}\left[\frac{\sinh(r-\gamma/2)}{\sinh(r+\gamma/2)}\right]^{1/2}.$$

For $\gamma=2r$, the two critical points denoted (R_{0+},θ_+) coalesce with the origin and all other nonzero critical points coalesce in pairs so that for $\gamma>2r$ the origin is the only critical point. As for the undamped case, (R_{n-},θ_-) are unstable saddle-type critical points. The critical points (R_{n+},θ_+) are stable for $P(n,r,\gamma)<2$ and unstable (saddlelike) for $P(n,r,\gamma)>2$, where

$$P(n,r,\gamma)=\left[2n\pi\pm\cos^{-1}\left[\frac{\cosh(\gamma/2)}{\cosh(r)}\right]\right]\cdot\times\frac{\sqrt{\sinh(r-\gamma/2)\sinh(r+\gamma/2)}}{\cosh(\gamma/2)}.$$

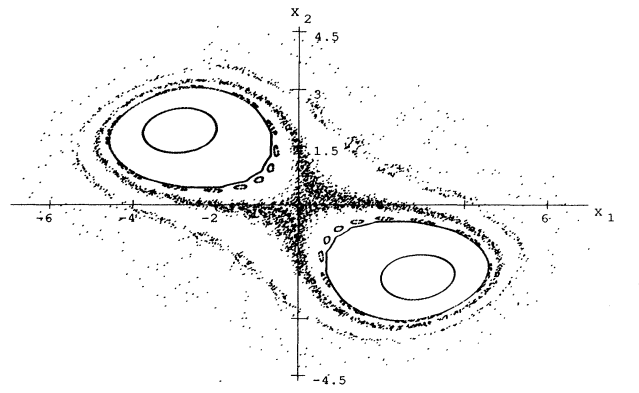

FIG. 3. Phase portrait of the classical map in the absence of dissipation. $g=1.5, \mu=0.01\pi$.

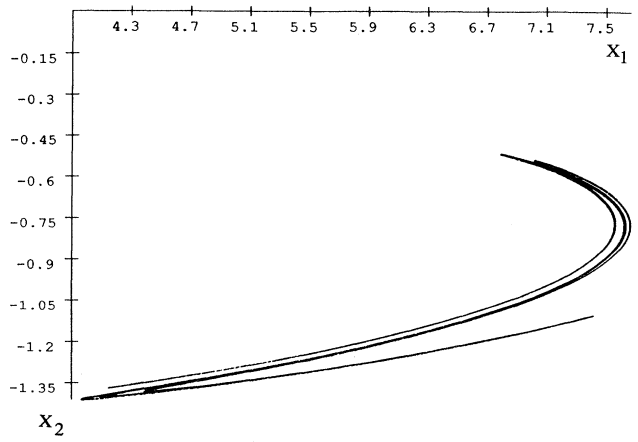

FIG. 4. Phase portrait of the classical map. $g=3.35$, $\mu=0.01\pi$, $\gamma=0.914$.

However, (R_{n+},θ_+) are now asymptotically stable (spirals or nodes) when stable and their domains of attraction divide up the phase space.

In Fig. 4 we plot the phase portrait in the case of large gain ($g=3.35$), and moderately large damping. This picture seems to indicate the presence of a strange attractor and consequently we see a transition to a dissipative chaotic motion. In Figs. 5(a)–5(c) and 6(a)–6(c) we plot the mean energy $\langle X_1^2+X_2^2\rangle$ for an initial uniform circular distribution of points. The radius of this distribution is chosen to be 0.5, to give variances for the phase-space variables equal to that for a quantum system prepared in a coherent state, that is, 0.25, in order that a comparison may be made with the quantum evolution in the following section. This means an initial circular distribution centered on the origin will have a mean energy of 0.5. In Fig. 5(a) the initial distribution is centered on the origin and there is no dissipation. After some initial oscillations the mean settles down to a steady-state value somewhere near the energy corresponding to the two critical points close to the origin. What appears to happen is that the distribution, initially centered on the saddle point at the origin, splits into two parts with each part drawn onto annular regions surrounding the critical points. The distribution is probably doubly peaked and uniformly distributed around each of these critical points. In Fig. 6(a) the initial distribution is centered on $\alpha=(1,0)$, which is in the chaotic region surrounding the origin when $g=1.5$. Again there is an initial oscillation of the mean energy, this time at a higher frequency, followed by a steady state that appears to diffuse slowly in energy. We have only taken the evolution out to 200 kicks in this case, as for larger times some points escape to the unbounded region leading to an error in the numerical evaluation of the energy. When dissipation is included, the critical points near the origin become attractors. Now the distribution is pulled on to the critical points and the mean energy approaches a new steady state, which is the mean energy of each of the two attracting points. This behavior is shown in Figs. 5(b), 5(c), 6(b), and 6(c) for various values of the damping constant.

III. QUANTUM DYNAMICS

To include the effect of dissipation in the quantum model, we must proceed a little differently to the classical case. It is not simply a matter of inserting a decay term in the Heisenberg equations, analogous to the last term in Eq. (2.1). In the quantum case the fluctuations, which necessarily accompany dissipation, must be correctly accounted for in order to preserve the commutation relations for the system operators. To include the effect of dissipation on the quantum dynamics between the kicks, we assume that the intracavity field mode is coupled to a zero-temperature heat bath. Standard techniques may then be used to derive a master equation for the field density operator. This equation may be solved over the time between kicks. The resulting density matrix is then subjected to the unitary transformation describing the kick and the master equation solved again with the post-kick

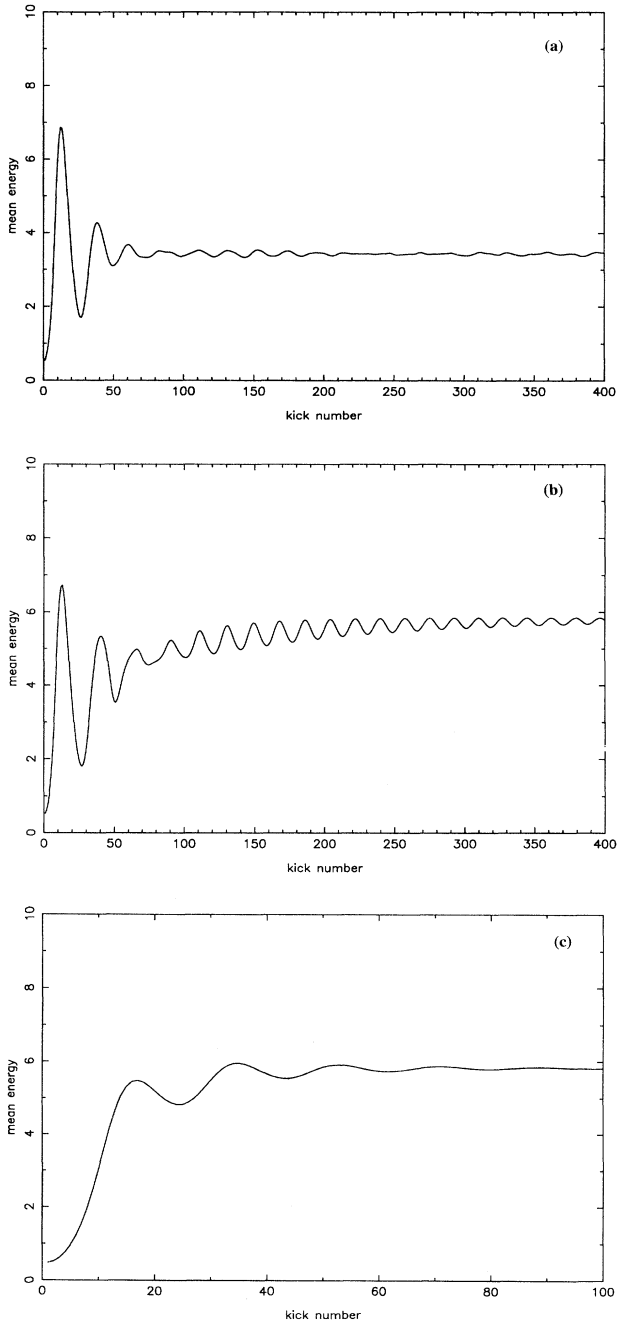

FIG. 5. Classical mean energy for an initial circular distribution of points at the origin. In all cases $\mu=0.01\pi, g=1.2$: (a) $\gamma=0$, (b) $\gamma=0.01$, (c) $\gamma=0.1$.

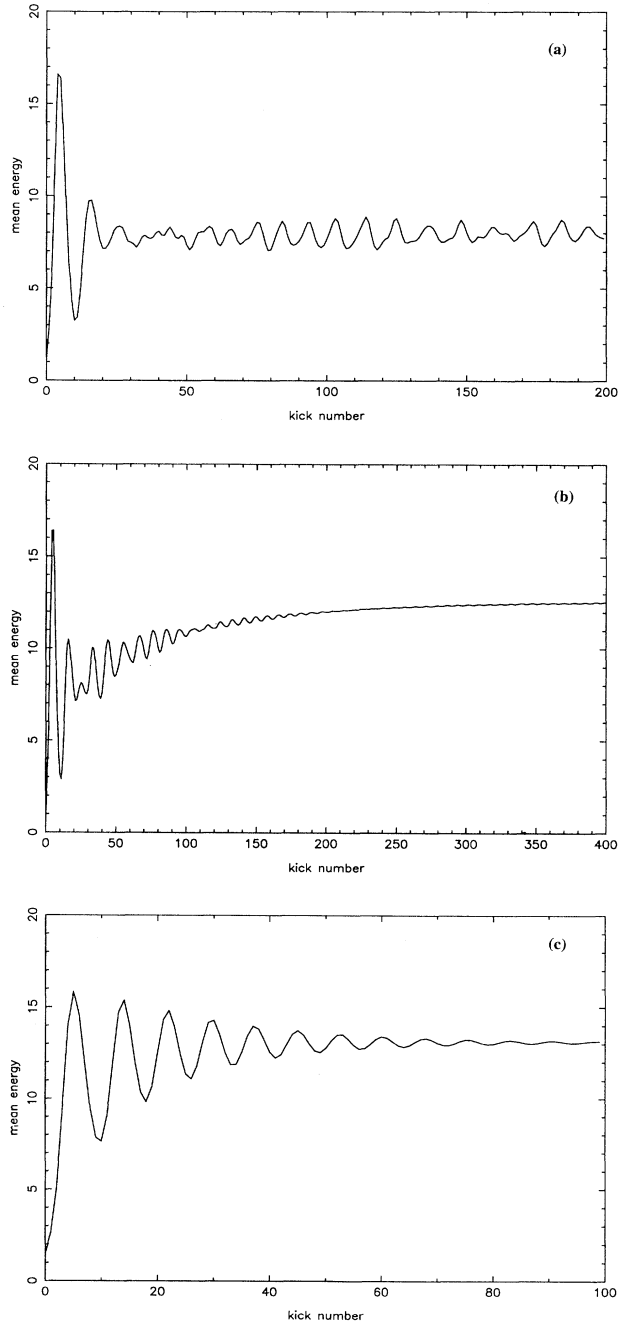

FIG. 6. Classical mean energy for an initial circular distribution centered at (1,0). In all cases $\mu=0.01\pi, g=1.5$: (a) $\gamma=0$, (b) $\gamma=0.01$, (c) $\gamma=0.1$.

density matrix as the initial condition. The process is then iterated.

Between the kicks the master equation is

$$\frac{d\rho}{dt}=-i\frac{\mu}{2}[(a^\dagger)^2a^2,\rho]+\frac{\gamma}{2}(2a\rho a^\dagger-a^\dagger a\rho-\rho a^\dagger a)\ . \tag{3.1}$$

If $\rho(t)$ is the density operator just after the kick applied at time t, the matrix elements of the density operator in the number basis a time τ later is given by [10]

$$\langle p|\rho(t+\tau)|q\rangle=\exp\left[i\frac{\theta}{2}(p-q)\right]f(\tau)^{(p+q)/2}(p!q!)^{-1/2}\times\sum_{n=p}^{\infty}\langle n|\rho(t)|n-(p-q)\rangle\times\{n![n-(p-q)]!\}^{1/2}\times\frac{(1+i\delta)^{-(n-p)}}{(n-p)!}[1-f(\tau)]^{(n-p)}\ ,$$

where

$$\delta=\frac{(p-q)}{\kappa}\ , \tag{3.2}$$

$$\kappa=\frac{\gamma}{\chi}\ , \tag{3.3}$$

$$\theta=\chi\tau\ , \tag{3.4}$$

$$f(\tau)=\exp[-\kappa\theta-i\theta(p-q)]\ . \tag{3.5}$$

In what follows we always choose $\tau=1$. At each kick the matrix elements transform as

$$\langle p|\rho'(t+\tau)|q\rangle=\sum_{n,m=0}^{\infty}U_{pn}\langle n|\rho(t+\tau)|m\rangle U_{qm}^*\ , \tag{3.6}$$

where

$$U_{mn}=\langle m|\exp\left[\frac{r}{2}[(a^\dagger)^2-a^2]\right]|n\rangle\ . \tag{3.7}$$

This unitary matrix element is zero if $m-n$ is odd, otherwise the explicit form is given in Ref. [7]. Of particular interest in this paper are the moments of the intracavity photon number,

$$\bar{n}^r=\sum_{n=0}^{\infty}n^r p_{nn}\ , \tag{3.8}$$

where the photon-number distribution p_{nn} is given by $p_{nn}=\langle n|\rho|n\rangle$. Of course in determining these moments numerically the infinite sums must be truncated. The truncation number must be chosen sufficiently large so that the trace of the density operator is very close to unity (within 1% was found to be satisfactory). The initial states were taken to be coherent states $|\alpha\rangle$, which have a reasonable semiclassical limit and are defined by the number state expansion

$$|\alpha\rangle=\exp(-|\alpha|^2)\sum_{n=0}^{\infty}\frac{\alpha^n}{\sqrt{n!}}|n\rangle\ . \tag{3.9}$$

Of special interest is the case where the cavity is initially unexcited for which $\alpha=0$.

The case of zero dissipation has been treated elsewhere [7], however, for completeness this case is illustrated in Figs. 7(a) and 8(a). The parameters have been chosen to correspond to those taken in the classical phase portraits. In all cases $\mu=0.01\pi$. Figure 7(a) depicts the mean photon number versus kick number for an initial vacuum state when the phase space near the origin is dominated by regular trajectories. Whereas the classical prediction

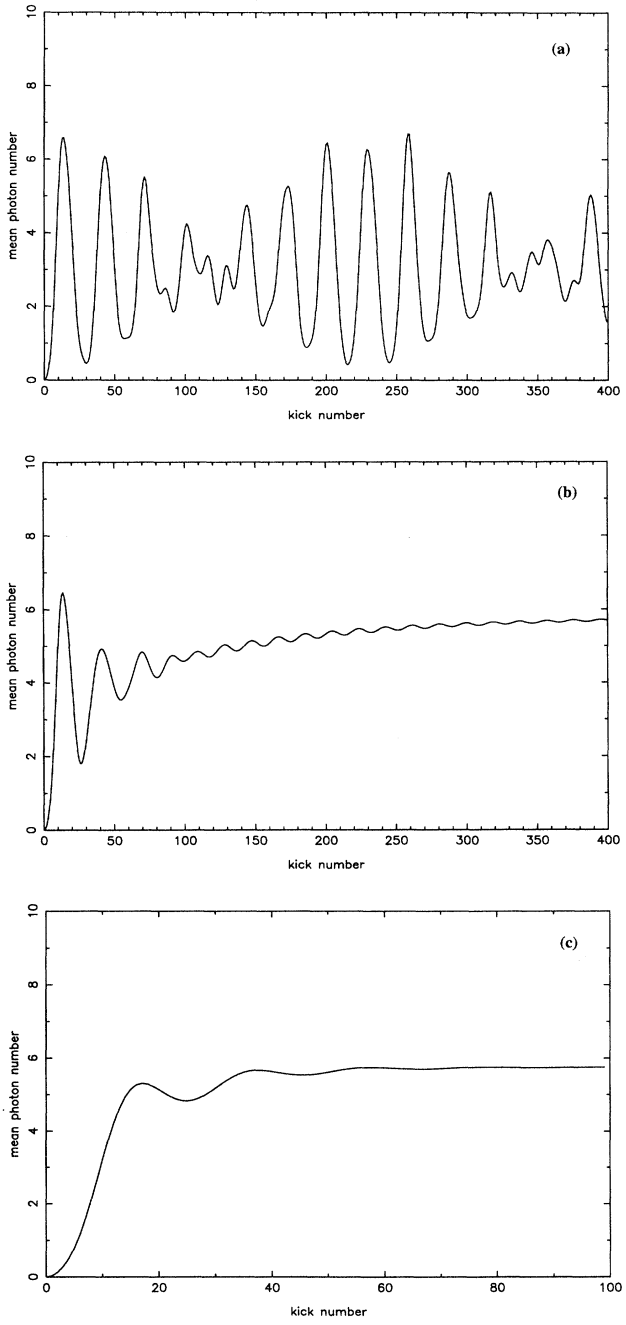

FIG. 7. Quantum mean photon number for the parameters in Figs. 5(a)–5(c).

for the mean energy in the cavity approaches a steady state [Fig. 5(a)], the quantum prediction deviates from this except on a very short time scale, giving a regular sequence of collapses and revivals. The revivals are a peculiarly quantum feature and reflect the underlying quantum coherence between quasienergy eigenstates preserved under unitary evolution. In Fig. 8(a) we change the parametric gain to access a region where classically there is chaotic behavior near the origin. The initial state was taken to be $\alpha=1$, which is localized in the chaotic region. Once again the quantum prediction for the mean intensity only follows the classical mean for short times [cf. Fig. 6(a)]. Now the departure from the classical result is characterized by a highly irregular recurrence sequence. Such an irregular revival sequence was also observed in the chaotic region of the kicked top [5]. The transition from a regular revival sequence to an irregular sequence is a quantum reflection of the corresponding transition to chaotic behavior in the classical model. It is evident in these figures that the quantum and classical results differ by 0.5 at the initial point. This is an artifact of the way in which we have chosen an initial classical distribution, which is meant to correspond in some way to the initial quantum states. In Fig. 7(a) the initial mean photon number is zero as the system starts from the vacuum state, however the classical result, Fig. 5(a), starts at 0.5, which is the sum of the initial phase-space variances. Nonetheless, for large photon numbers the quantum and classical results are quite close to each other. This is the required semiclassical limit in the model as $\hbar$ has been set equal to unity and thus we feel justified in choosing the particular initial classical distribution.

The effect of damping is depicted in Figs. 7(b), 7(c), 8(b), and 8(c). The general feature is that it takes only a relatively small amount of damping to destroy the quantum revivals, be they regular or irregular, and restore the classically expected approach to the steady state. How-

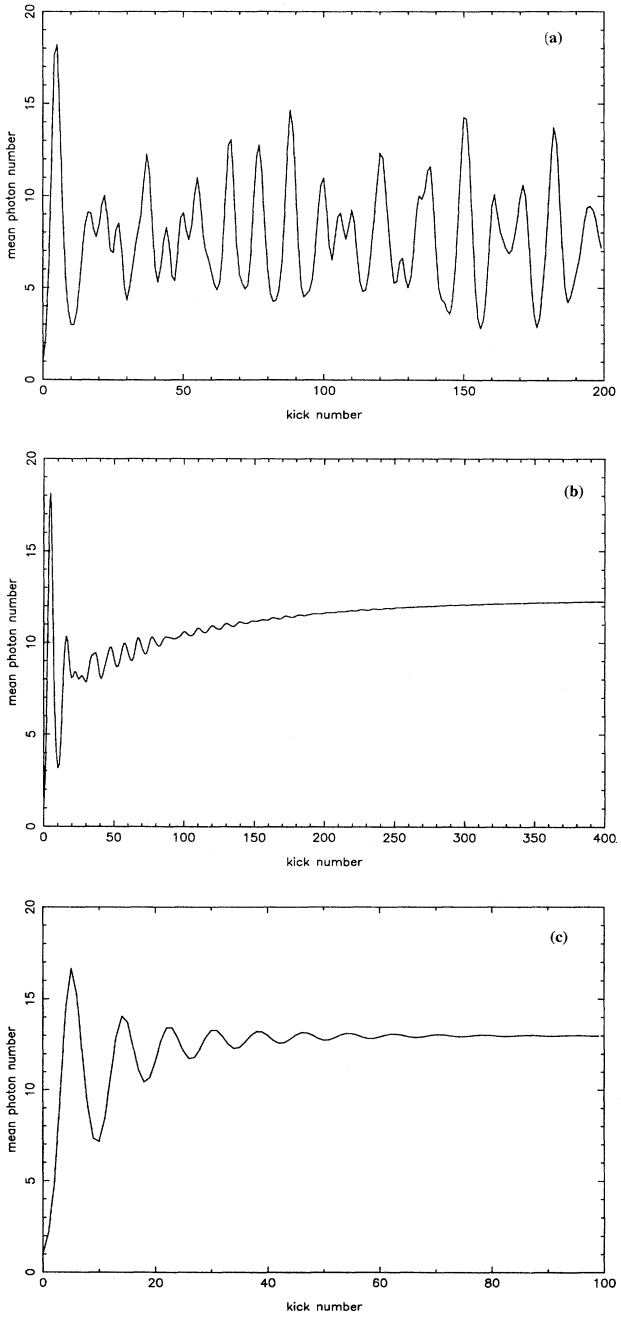

FIG. 8. Quantum mean photon number for the parameters in Figs. 6(a)–6(c).

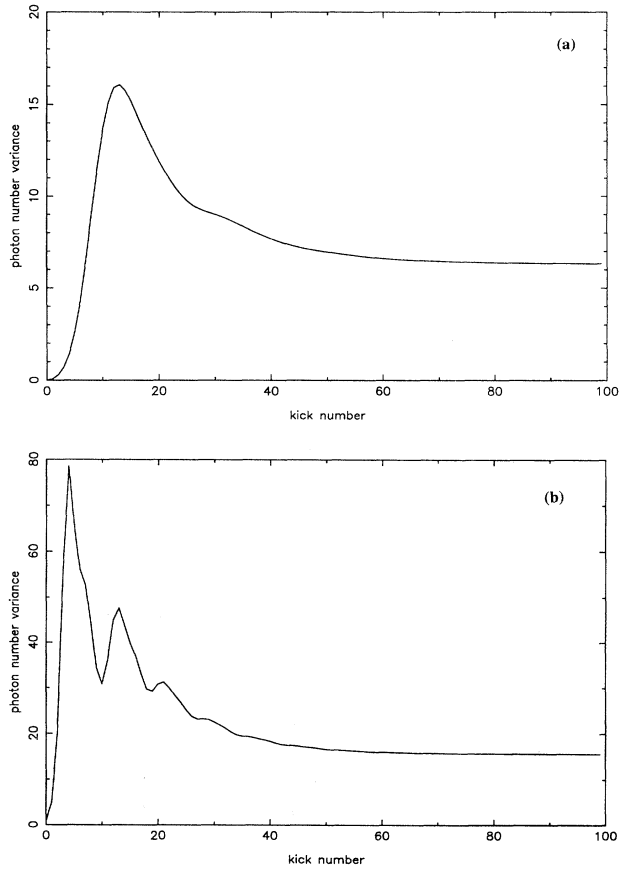

FIG. 9. Quantum photon number variance where $\gamma=0.1$: (a) $g=1.2$, (b) $g=1.5$.

ever, there are some small differences that can probably be attributed to the fact that an initial uniform distribution of points in the classical model is not a perfect representation of the quantum state. However, the agreement between the classical and quantum results is quite impressive.

In Figs. 9(a) and 9(b) we plot the photon-number variance versus kick number for the case of $\gamma=0.1$. Comparison with the steady-state photon number reached in Fig. 7(c) indicates that the steady state of the device is quite close to a coherent state. The agreement between the mean and variance is best for the regular region. Thus this device produces a continuous-wave steady state with near shot-noise-limited intensity fluctuations. In fact, the steady-state phase-space distribution is probably double peaked, each peak centered on each of the stable fixed points close to the origin. Overall the device has converted a pulsed field to a continuous-wave field at half the frequency with a well-defined intensity and phase defined up to a π phase shift. Further investigations of the quantum statistical properties of the steady state are in progress.

IV. DISCUSSION AND CONCLUSION

We have shown how the different quantum and classical dynamics of a classically chaotic system become similar when weak dissipation is present. Furthermore, this model is realistic enough to be subjected to an experimental test [7]. The gain parameters used in this paper are relatively modest corresponding to squeezing of between 30% and 56%. These values have been achieved experimentally [9]. The nonlinear phase-shift parameter μ is a scale parameter and fixes the photon-number scale of the model. Typical values of μ (10^{-17}) would lead to quite large photon numbers but possibly within reach of a pulsed pump field.

There have been a number of papers recently discussing the effect of measurement on the quantum features of a classically chaotic system [13–15]. The model of this paper is in fact an example of how monitoring a nonlinear quantum system may restore classical behavior. In our model it is necessary to measure the photon number continuously. This is usually done by a demolition counting scheme in which the photon detection process represents a linear loss term from the cavity. This linear loss is well modeled at optical frequencies by precisely the master equation of Eq. (3.1). (See, for example, Ref. [16] and references therein.) Thus we conclude that the effect of measurement is to modify both the quantum and classical dynamics but that the predictions of both models are arbitrarily close the more closely (that is the larger is γ) the system is monitored. Of course there may be other forms of number measurements based on quantum nondemolition schemes that do not have as much of an effect on the quantum dynamics. We are currently investigating the application of such schemes to the model of this paper.

[1] G. Casati, B. V. Chirikov, J. Ford, and F. M. Izrailev, in *Stochastic Behavior in Classical and Quantum Hamiltonian Systems,* edited by G. Casati and J. Ford (Springer, Berlin, 1979).
[2] D. L. Shepelyansky, Physica (Amsterdam) **23** D, 103 (1987).
[3] S. Fishman, D. R. Grempel, and R. E. Prange, Phys. Rev. Lett. **49**, 49 (1982).
[4] M. V. Berry and M. Tabor, Proc. R. Soc. London Ser. A **356**, 375 (1977).
[5] F. Haake, M. Kus, and R. Scharf, Z. Phys. B **65**, 381 (1987).
[6] J. E. Bayfield, G. Casati, I. Guarneri, and D. W. Sokol, Phys. Rev. Lett. **63**, 364 (1989).
[7] G. J. Milburn, Phys. Rev. A **41**, 6567 (1990).
[8] P. D. Drummond and D. F. Walls. J. Phys. A **13**, 725 (1980).
[9] See the special issue on squeezed states, J. Opt. Soc. Am. B **4**, 1715 (1989).
[10] G. J. Milburn and C. A. Holmes, Phys. Rev. Lett. **56**, 2237 (1986).
[11] G. J. Milburn, Phys. Rev. A **33**, 674 (1986).
[12] A. J. Lichtenberg and M. A. Liberman, *Regular and Stochastic Motion* (Springer, New York 1986).
[13] R. Grobe and F. Hakke, Z. Phys. B **68**, 503 (1987).
[14] B. C. Sanders and G. J. Milburn, Z. Phys. B **77**, 497 (1989).
[15] T. Dittrich and R. Graham, Phys. Rev. A **42**, 4647 (1990).
[16] C. A. Holmes, G. J. Milburn, and D. F. Walls, Phys. Rev. A **39**, 2493 (1989).